

UCLA

UCLA Previously Published Works

Title

Effective optical properties of absorbing nanoporous and nanocomposite thin films

Permalink

<https://escholarship.org/uc/item/1gr8n7m2>

Journal

Journal of Applied Physics, 101(1)

ISSN

0021-8979

Authors

Garahan, A
Pilon, L
Yin, J
[et al.](#)

Publication Date

2007

Peer reviewed

1 Effective optical properties of absorbing nanoporous 2 and nanocomposite thin films

3 Anna Garahan, Laurent Pilon,^{a)} and Juan Yin
4 *Mechanical and Aerospace Engineering Department, Henry Samueli School of Engineering
5 and Applied Science, University of California, Los Angeles, California 90095*

6 Indu Saxena
7 *Intelligent Optical Systems, Inc., Torrance, California 90505*

8 (Received 23 June 2006; accepted 12 October 2006)

9 This paper aims at developing numerically validated models for predicting the through-plane
10 effective index of refraction and absorption index of nanocomposite thin films. First, models for the
11 effective optical properties of such materials are derived from previously reported analysis applying
12 the volume averaging theory (VAT) to Maxwell's equations. The transmittance and reflectance of
13 nanoporous thin films are computed by solving Maxwell's equations and the associated boundary
14 conditions at all interfaces using finite element methods. The effective optical properties of the films
15 are retrieved by minimizing the root mean square of the relative errors between the computed and
16 theoretical transmittance and reflectance. Nanoporous thin films made of SiO₂ and TiO₂ consisting
17 of cylindrical nanopores and nanowires are investigated for different diameters and various
18 porosities. Similarly, electromagnetic wave transport through dielectric medium with embedded
19 metallic nanowires are simulated. The numerical results are compared with predictions from widely
20 used effective property models including (1) the Maxwell-Garnett theory, (2) the Bruggeman
21 effective medium approximation, (3) the parallel, (4) series, (5) Lorentz-Lorenz, and (6) the VAT
22 models. Very good agreement is found with the VAT model for both the effective index of refraction
23 and absorption index. Finally, the effect of volume fraction on the effective index of refraction and
24 absorption index predicted by the VAT model is discussed. For certain values of wavelengths and
25 volume fractions, the effective index of refraction or absorption index of the composite material can
26 be smaller than that of both the continuous and dispersed phases. These results indicate guidelines
27 for designing nanocomposite materials with desired optical properties. © 2006 American Institute of
28 Physics. [DOI: 10.1063/1.2402327]
29

30 I. INTRODUCTION

31 In recent years, synthesis and characterization of nano-
32 composite thin films in general and nanoporous in particular,
33 have been the subject of intense study.¹⁻⁴ Potential applica-
34 tions include dye-sensitized solar cells,⁵⁻⁷ low-k dielectric
35 materials,^{8,9} biosensors,¹⁰⁻¹² and optical devices including
36 waveguides,¹³⁻¹⁵ Bragg reflectors and Fabry-Perot
37 filters.¹⁶⁻²² For example, in order to confine and propagate
38 electromagnetic waves within a waveguide, the guide region
39 itself must have a higher index of refraction than the sur-
40 rounding cladding.²³ On the other hand, Bragg reflectors and
41 Fabry-Perot filters are built by generating alternating layers
42 with prescribed thickness and index of refraction. This ge-
43 ometry uses constructive and destructive interferences to se-
44 lectively reflect or transmit at desired wavelengths. In each
45 of these optical applications, the index of refraction is tuned
46 by controlling the morphology and porosity of the nanosize
47 pores formed by electrochemical etching of silicon, for ex-
48 ample. Optimizing the performance of a given component
49 requires accurate knowledge of the effect of porosity, pore

shape and size as well as the optical properties of each phase
on the effective optical properties of the nanocomposite me-
dium.

Various effective property models have been proposed in
the literature and were discussed in our previous study.²⁴ In
brief, the Maxwell-Garnett theory (MGT)²⁵ was first devel-
oped to model the effective electric permittivity of heteroge-
neous media consisting of monodispersed spheres arranged
in a cubic lattice structure within a continuous matrix and of
diameter much smaller than the wavelength of the incident
electromagnetic (EM) wave. Then, the effective dielectric
constant $\epsilon_{r,\text{eff}}$ is expressed as

$$\epsilon_{r,\text{eff}} = \epsilon_{r,c} \left[1 - \frac{3\phi(\epsilon_{r,c} - \epsilon_{r,d})}{2\epsilon_{r,c} + \epsilon_{r,d} + \phi(\epsilon_{r,c} - \epsilon_{r,d})} \right], \quad (1)$$

where $\epsilon_{r,c}$ and $\epsilon_{r,d}$ are the dielectric constant of the continu-
ous and dispersed phases, respectively, while ϕ is the poros-
ity. For dispersed phase volume fractions larger than $\pi/6$
 $\approx 52\%$ and polydispersed spheres the Bruggeman²⁶ model
gives the following implicit equation for $\epsilon_{r,\text{eff}}$:

^{a)}Telephone: (310)-206-5598; Fax: (310)-206-4830. Electronic mail:
pilon@seas.ucla.edu

$$1 - \phi = \frac{\left(\frac{\epsilon_{r,\text{eff}} - \epsilon_{r,d}}{\epsilon_{r,c}} \right)}{\left[\left(\frac{\epsilon_{r,\text{eff}}}{\epsilon_{r,c}} \right)^{1/3} \left(1 - \frac{\epsilon_{r,d}}{\epsilon_{r,c}} \right) \right]} \quad (2)$$

69 On the other hand, the Lorentz-Lorenz model gives the ef-
70 fective index of refraction n_{eff} as

$$\left(\frac{n_{\text{eff}}^2 - 1}{n_{\text{eff}}^2 + 2} \right) = (1 - \phi) \left(\frac{n_c^2 - 1}{n_c^2 + 2} \right) + \left(\phi \frac{n_d^2 - 1}{n_d^2 + 2} \right), \quad (3)$$

72 where n_c and n_d are the index of refraction of the continuous
73 and dispersed phases, respectively. Alternatively, the parallel
74 model gives the effective property ψ_{eff} as a linear function of
75 the properties of the continuous and dispersed phases, i.e.,

$$\psi_{\text{eff}} = (1 - \phi)\psi_c + \phi\psi_d. \quad (4)$$

77 The series model, on the other hand, is expressed as

$$\frac{1}{\psi_{\text{eff}}} = \frac{1 - \phi}{\psi_c} + \frac{\phi}{\psi_d}. \quad (5)$$

79 In addition, del Rio *et al.*²⁷ suggested the following effective
80 model for electrical conductivity based on the reciprocity
81 theorem

$$\sigma_{\text{eff}} = \sigma_c \frac{1 + \phi(\sqrt{\sigma_c/\sigma_d} - 1)}{1 + \phi(\sqrt{\sigma_d/\sigma_c} - 1)}. \quad (6)$$

83 Recently, del Rio and Whitaker^{28,29} applied the volume av-
84 eraging theory (VAT) to Maxwell's equations for an en-
85 semble of dispersed domains of arbitrary shape in a continu-
86 ous matrix. They predicted the effective dielectric constant
87 $\epsilon_{r,\text{eff}}$, relative permeability $\mu_{r,\text{eff}}$, and electrical conductivity
88 σ_{eff} of a two-phase mixture as²⁸

$$\epsilon_{r,\text{eff}} = (1 - \phi)\epsilon_{r,c} + \phi\epsilon_{r,d}, \quad (7)$$

$$1/\mu_{r,\text{eff}} = (1 - \phi)/\mu_{r,c} + \phi/\mu_{r,d}, \quad (8)$$

$$\sigma_{\text{eff}} = (1 - \phi)\sigma_c + \phi\sigma_d. \quad (9)$$

92 The range of validity of these expressions was discussed in
93 details, and a set of inequalities to be satisfied was developed
94 by del Rio and Whitaker.²⁸ Their model has been numeri-
95 cally validated by Braun and Pilon²⁴ for the effective
96 through-plane index of refraction of *nonabsorbing* nano-
97 porous media with open and closed cylindrical nanopores of
98 various shapes and sizes corresponding to a wide range of
99 porosity. The other models, however, underpredicted the nu-
100 merical results.²⁴

101 Moreover, validation of the above models against experi-
102 mental data often yields contradictory results.³⁰ These con-
103 tradictions can be attributed to the fact that first, some of
104 these models were not developed for the index of refraction
105 but for the dielectric constant. However, they have been used
106 for optical properties (e.g., Refs. 8, 9, 31, and 13). Second,
107 unlike the present study, some of these models have also
108 been derived by considering a unit cell containing one pore
109 with uniform incident electromagnetic fields thus ignoring
110 possible interference taking place between adjacent
111 pores.^{25,26,32} Finally, large experimental uncertainty may ex-

ist in the measure of the porosity and the retrieval of the **112**
complex index of refraction from transmittance and reflec- **113**
tance measurements. The latter is very sensitive to the sur- **114**
face roughness of the film and to the uniformity and value of **115**
the film thickness. Unfortunately, often, neither the film **116**
thickness L nor the experimental uncertainty for both ϕ and **117**
 m_{eff} are reported. **118**

The present study extends our previous investigation to **119**
absorbing nanocomposite thin films. It aims at modeling **120**
both the through-plane effective index of refraction and ab- **121**
sorption index of (1) nanoporous thin films consisting of **122**
horizontally aligned cylindrical nanopores or nanowires with **123**
different diameters and various porosities and of (2) dielec- **124**
tric medium with embedded metallic nanowires. Such thin **125**
films are anisotropic and this study focuses on properties in **126**
the direction normal to the film surface. It is limited to non- **127**
magnetic materials for which $\mu_{r,c} = \mu_{r,d} = \mu_{r,\text{eff}} = 1$. Spectral **128**
normal-normal transmittance and reflectance are obtained by **129**
numerically solving Maxwell's equations and used to re- **130**
trieve the effective index of refraction and absorption index. **131**
The numerical results are then compared with previously re- **132**
viewed models. Finally, the VAT model is analyzed in de- **133**
tails. **134**

II. ANALYSIS **135**

A. Optical properties from volume averaging theory **136**

The index of refraction n and the absorption index k of **137**
homogeneous media can be expressed in terms of the real **138**
part of their dielectric constant ϵ_r and of their electrical con- **139**
ductivity σ as²³ **140**

$$n^2 = \frac{1}{2} \left[\epsilon_r + \sqrt{\epsilon_r^2 + \left(\frac{\lambda\sigma}{2\pi c_0 \epsilon_0} \right)^2} \right], \quad (10) \quad \mathbf{141}$$

$$k^2 = \frac{1}{2} \left[-\epsilon_r + \sqrt{\epsilon_r^2 + \left(\frac{\lambda\sigma}{2\pi c_0 \epsilon_0} \right)^2} \right], \quad (11) \quad \mathbf{142}$$

where λ is the wavelength of incident radiation, c_0 is the **143**
speed of light in vacuum, and ϵ_0 is the permittivity of free **144**
space. The expression derived by Del Rio and Whitaker²⁸ for **145**
the effective dielectric constant $\epsilon_{r,\text{eff}}$ and electrical conduc- **146**
tivity σ_{eff} of a two-phase medium [Eqs. (7) and (9)] can be **147**
used to derive the effective optical properties of a two-phase **148**
nanocomposite material **149**

$$n_{\text{eff}}^2 = \frac{1}{2} [A + \sqrt{A^2 + B^2}], \quad (12) \quad \mathbf{150}$$

$$k_{\text{eff}}^2 = \frac{1}{2} [-A + \sqrt{A^2 + B^2}], \quad (13) \quad \mathbf{151}$$

where **152**

$$A = \epsilon_{r,\text{eff}} = \phi(n_d^2 - k_d^2) + (1 - \phi)(n_c^2 - k_c^2) \quad (14) \quad \mathbf{153}$$

and **154**

$$155 \quad B = \frac{\lambda \sigma_{\text{eff}}}{2\pi c_0 \epsilon_0} = 2n_d k_d \phi + 2n_c k_c (1 - \phi). \quad (15)$$

156 In particular, when the dispersed phase is vacuum, $\epsilon_{r,d}=n_d$
 157 $=1$, and $k_d=\sigma_d=0$. Note also that, unlike other effective
 158 property models, the above VAT models for n_{eff} and k_{eff} de-
 159 pend on both the real and complex parts of the complex
 160 indices of refraction of the dispersed and continuous phases.
 161 In other words, R_{calc} and k_d affect not only k_{eff} but also n_{eff} .

162 **B. Governing equations and numerical**
 163 **implementation**

164 In order to develop the numerical model, let us first con-
 165 sider a surrounding environment (medium 1, $n_1, k_1=0$) from
 166 which an electromagnetic wave is incident on an absorbing
 167 thin film (medium 2, n_2, k_2) deposited onto an absorbing
 168 dense substrate (medium 3, n_3, k_3). A linearly polarized
 169 plane wave in transverse electric (TE) mode is incident nor-
 170 mal to the film top surface and propagates through the two-
 171 dimensional thin film along the x direction. As the wave
 172 propagates in the x - y plane, it has only one electric field
 173 component in the z direction, while the magnetic field has
 174 two components in the x - y plane (i.e., perpendicularly polar-
 175 ized), such that in a general time-harmonic form

$$176 \quad \vec{E}(x,y,t) = E_z(x,y)e^{i\omega t}\vec{e}_z, \quad (16)$$

$$177 \quad \vec{H}(x,y,t) = [H_x(x,y)\vec{e}_x + H_y(x,y)\vec{e}_y]e^{i\omega t}.$$

179 Here, \vec{E} is the electric field vector, \vec{H} is the magnetic field
 180 vector, $\vec{e}_x, \vec{e}_y,$ and \vec{e}_z are the unit vectors, and $\omega=2\pi c_0/\lambda$ is
 181 the angular frequency of the wave. For general time-varying
 182 fields in a conducting medium, Maxwell's equations can be
 183 written as

$$184 \quad \nabla \times \left[\frac{1}{\mu_r \mu_0} \nabla \times \vec{E}(x,y,t) \right] - \omega^2 \epsilon_r^* \epsilon_0 \vec{E}(x,y,t) = 0, \quad (17)$$

$$185 \quad \nabla \times \left[\frac{1}{\epsilon_r^* \epsilon_0} \nabla \times \vec{H}(x,y,t) \right] - \omega^2 \mu_r \mu_0 \vec{H}(x,y,t) = 0, \quad (18)$$

186 where μ_0 and μ_r are the magnetic permeability of vacuum
 187 and the relative magnetic permeability, respectively, while
 188 $\epsilon_r^* (=n^2 - k^2 - i2nk)$ is the complex dielectric constant. The
 189 associated boundary conditions are

$$190 \quad \vec{n} \times (\vec{H}_1 - \vec{H}_2) = 0 \quad (19)$$

191 at the surroundings-film interface,

$$192 \quad \vec{n} \times \vec{H} = 0 \quad (20)$$

193 at symmetry boundaries,

$$194 \quad \sqrt{\mu_r \mu_0} (\vec{n} \times \vec{H}) + \sqrt{\epsilon_0 \epsilon_r^*} \vec{E} = 0 \quad (21)$$

195 at the film-substrate interface, and

$$196 \quad \sqrt{\mu_0 \mu_r} (\vec{n} \times \vec{H}) + \sqrt{\epsilon_0 \epsilon_r^*} \vec{E} = 2\sqrt{\epsilon_0 \epsilon_r^*} \vec{E}_0, \quad (22)$$

197 at the source surface, where \vec{n} is the normal vector to the
 198 appropriate interface. Equation (21) corresponds to the im-

pedance boundary condition for a semi-infinite substrate 199
 while Eq. (22) is the low reflecting boundary condition to 200
 model the imaginary source surface where the incident elec- 201
 tromagnetic wave $\vec{E}_0=E_0\vec{e}_z$ is emitted and that is transparent 202
 to the reflected waves. 203

Moreover, the Poynting vector $\vec{\pi}$ is defined as the cross 204
 product of the electric and magnetic vectors, $\vec{\pi}=\frac{1}{2}\text{Re}\{\vec{E} \times \vec{H}\}$. Its magnitude corresponds to the energy flux carried 205
 by the propagating electromagnetic wave. Averaging the x 206
 component of the Poynting vector at location (x,y) over a 207
 period $2\pi/\omega$ of the EM wave gives²³ 208
 209

$$|\pi_x|_{\text{avg}}(x,y) = -\frac{1}{2}\text{Re}\{E_z H_y^*\} \quad 210$$

and 211

$$|\pi_y|_{\text{avg}}(x,y) = \frac{1}{2}\text{Re}\{E_z H_x^*\}. \quad (23) \quad 212$$

The $H_x(x,y)\vec{e}_x + H_y(x,y)\vec{e}_y$ incident electric field $\vec{E}_0=E_0z\vec{e}_z$ 213
 and, therefore, the incident time-averaged Poynting vector 214
 $|\vec{\pi}_0|_{\text{avg}}$ are imposed at all locations along the source surface. 215
 The values of the x component of the Poynting vector along 216
 the film-substrate interface are then calculated numerically 217
 and averaged along the boundary to yield $|\pi_{x,t}|_{\text{avg}}$. The trans- 218
 mittance of the thin film is then recovered by taking the ratio 219
 of the transmitted film to the incident average Poynting vec- 220
 tors, i.e., $T_{\text{num}}=|\pi_{x,t}|_{\text{avg}}/|\pi_{x,0}|_{\text{avg}}$. Similarly, the magnitude of 221 **AQ:**
 the x component of the reflected time-averaged Poynting **#2**
 vector $|\pi_{x,r}|_{\text{avg}}$ is computed numerically, and the reflectance 222
 of the film is computed according to $R_{\text{num}}=|\pi_{x,r}|_{\text{avg}}/|\pi_{x,0}|_{\text{avg}}$. 223

Finally, the above equations were solved numerically us- 225
 ing a commercially available finite element solver (FEMLAB 226
 3.0) applying the Galerkin finite element method on unstruc- 227
 tured meshes. The two-dimensional (2D) Maxwell equations 228
 are solved in the frequency domain using a 2D transverse 229
 electric (TE) wave formulation as described by Eq. (16). In 230
 particular, the discretization uses second-order elements to 231
 solve for the electric field.³³ 232

In order to validate the numerical implementation of this 233
 system of equations, a system composed of a dense absorb- 234
 ing thin film ($n_2=1.7, k_2$) of thickness L deposited on a per- 235
 fectly reflective substrate ($n_3=k_3 \rightarrow \infty$) in air ($n_1=1, k_1=0$) 236
 was simulated. The value of k_2 was varied over three orders 237
 of magnitude from 0.001 to 1, and the infinitely large optical 238
 constants of the substrate were imposed as $n_3=k_3=10^6$. Nor- 239
 mal reflectivity of the system was computed and plotted as a 240
 function of $\pi L/\lambda$.³⁰ The numerical solutions match the ana- 241
 lytical solutions found in Ref. 23, for example. 242

Figure 1 schematically shows the geometry of the simu- 243
 lated nanocomposite thin film on a semi-infinite substrate. 244
 The Maxwell equations are solved in both phases separately 245
 as previously described. Equation (19) is used as the bound- 246
 ary condition not only at the incident vacuum-film interface 247
 but also at all continuous/dispersed phase interfaces. Figure 1 248
 is a schematic representation of an actual model consisting of 249
 three nanopores or nanowires of diameter $D=10$ nm and cell 250
 width H of 20 nm corresponding to a volume fraction ϕ 251
 $=\pi D^2/4H^2=0.1963$. Figure 1 also indicates material proper- 252

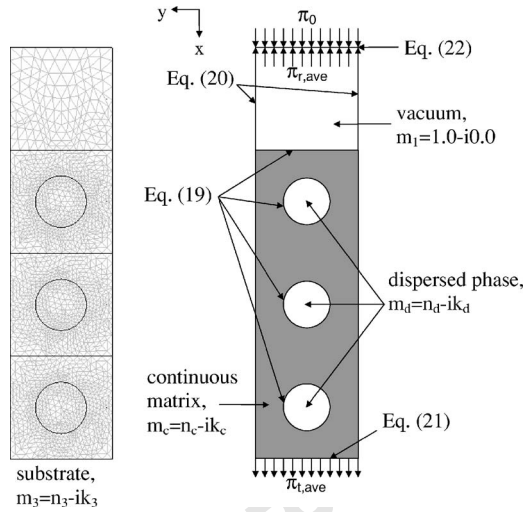


FIG. 1. Schematic of the physical model and the corresponding finite element grid of the absorbing nanoporous thin film along with the boundary conditions.

waves are not observed in the current situation as resonance modes were not excited for the materials and wavelengths considered. Finally, we assume that all interfaces are optically smooth, i.e., surface roughness is much smaller than the wavelength of the incident EM wave. This assumption may not be satisfied in practice and scattering by the sometimes rough film surface can be observed.³⁴⁻³⁶

The Microsoft Excel Solver based on the generalized reduced gradient nonlinear optimization method³⁷ was used to identify the optimum n_{eff} and k_{eff} that minimizes the root mean square δT and δR . The theoretical transmittance and reflectance for homogeneous thin films under normal incidence are expressed as³⁸

$$T_{\text{calc}}(\lambda) = \frac{\tau_{12}\tau_{23}e^{-\kappa_2 L}}{1 + 2r_{12}r_{23}e^{-\kappa_2 L} \cos(\delta_{12} + \delta_{23} - \zeta_2) + r_{12}^2 r_{23}^2 e^{-2\kappa_2 L}}, \quad (25)$$

$$R_{\text{calc}}(\lambda) = \frac{r_{12}^2 + 2r_{12}r_{23}e^{-\kappa_2 L} \cos(\delta_{12} + \delta_{23} - \zeta_2) + r_{23}^2 e^{-2\kappa_2 L}}{1 + 2r_{12}r_{23}e^{-\kappa_2 L} \cos(\delta_{12} + \delta_{23} - \zeta_2) + r_{12}^2 r_{23}^2 e^{-2\kappa_2 L}}, \quad (26)$$

where

$$r_{ij}^2 = \frac{(n_i - n_j)^2 + (k_i - k_j)^2}{(n_i + n_j)^2 + (k_i + k_j)^2}, \quad \tau_{ij} = \frac{n_i}{n_j} \frac{4(n_i^2 + k_i^2)}{(n_i + n_j)^2 + (k_i + k_j)^2},$$

$$\tan \delta_{ij} = \frac{2(n_i k_j - n_j k_i)}{n_i^2 + k_i^2 - (n_j^2 + k_j^2)}, \quad \kappa_2 = 4\pi k_2 / \lambda, \quad \text{and} \quad \zeta_2 = 4\pi n_2 / \lambda. \quad (27)$$

Here, the subscripts 1 and 3 refer to the media above and below the nanocomposite thin film treated as an effective homogeneous and referred to by subscript 2. Validation of the retrieval method combined with the numerically computed transmittance was performed by simulating a dense silicon absorbing thin film of thickness $L=1 \mu\text{m}$ surrounded on both sides by vacuum ($n_1=n_3=1.0$, $k_1=k_3=0.0$) and having a constant complex index of refraction $m_2=n_2-ik_2=3.5-i0.01$ over the spectral interval from 440 to 1700 nm. The values of n_2 and k_2 retrieved with the above mentioned optimization method fall within $9.0 \times 10^{-6}\%$ and 0.06% of the input values, respectively. Therefore, both the numerical simulation tool and the inverse method to retrieve the effective complex index of refraction of nanocomposite thin films from transmittance and reflectance calculations have been validated and can now be used.

IV. RESULTS AND DISCUSSION

A. Absorbing nanoporous media

Simulations of electromagnetic wave transport in nanoporous absorbing SiO_2 thin film were conducted for various porosities, film thicknesses, and pore shapes and sizes. First, the continuous phase was assumed to be characterized by constant optical properties $n_c=1.44$ and $k_c=0.01$ over the spectral range from 400 to 900 nm while $n_d=n_1=1.0$, $k_d=k_1=k_3=0.0$, and $n_3=3.39$. The optimization method previ-

ties of the different domains and the locations at which each of the boundary conditions are applied. Note that the lines separating two adjacent cubic cells do not correspond to an actual boundary conditions.

Finally, it is important to note that Maxwell's equations are generally applied to macroscopic averages of the fields which can vary widely in the vicinity of individual atoms where they undergo quantum mechanical effects. In addition, both the matrix and the nanodomains are treated as homogeneous and isotropic with index of refraction n and absorption index k equal to that of the bulk.

III. RETRIEVAL OF EFFECTIVE COMPLEX INDEX OF REFRACTION

The effective complex index of refraction of the nanocomposite thin film was retrieved by minimizing the root mean square of the relative error for the transmittance δT and reflectance δR defined as

$$\delta T^2 = \frac{1}{N} \sum_{i=1}^N \left[\frac{T_{\text{calc}}(\lambda_i) - T_{\text{num}}(\lambda_i)}{T_{\text{num}}(\lambda_i)} \right]^2 \quad \text{and} \quad (24)$$

$$\delta R^2 = \frac{1}{N} \sum_{i=1}^N \left[\frac{R_{\text{calc}}(\lambda_i) - R_{\text{num}}(\lambda_i)}{R_{\text{num}}(\lambda_i)} \right]^2,$$

where $T_{\text{num}}(\lambda_i)$ and $R_{\text{num}}(\lambda_i)$ are the transmittance and reflectance computed numerically using FEMLAB 3.0 while $T_{\text{calc}}(\lambda_i)$ and $R_{\text{calc}}(\lambda_i)$ are the transmittance and reflectance predicted from the electromagnetic wave theory at N different wavelengths λ_i between 400 and 900 nm.

In predicting the theoretical transmittance T_{calc} and reflectance R_{calc} from the EM wave theory, polarization effects are disregarded since (1) the incident EM wave is normal to the surface, i.e., the plane of incidence is not defined and the components of the polarization cannot be distinguished²³ and (2) scattering is neglected as the nanopores or nanowires are much smaller than the wavelength of the EM wave. In addition, nonlinear optical effects are neglected and surface

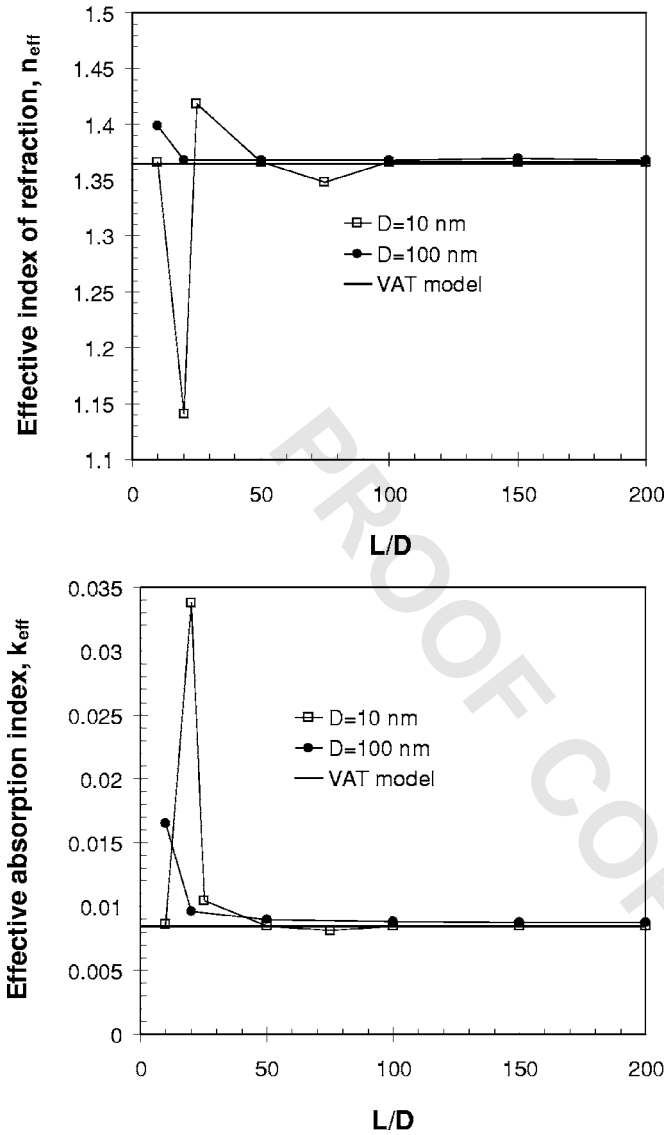


FIG. 2. Evolution of the through-plane effective index of refraction and absorption index of nanoporous SiO_2 thin films as a function of L/D for films with 19.63% porosity and pore diameters of 10 and 100 nm.

ously described was used to retrieve the through-plane effective index of refraction n_{eff} and absorption index k_{eff} from the numerically computed transmittance. A numerically converged solution was obtained with more than 50,000 triangular meshes for 250 wavelengths with a 2 nm increment. The pore diameter was 10 or 100 nm while the ratio of the film thickness L to pore diameter D varied from 10 to 200. Finally, for a given pore diameter, the porosity ϕ varied from 0.0 to 0.7 by changing the dimensions of the cubic cells.

Figure 2 shows the evolution of the through-plane effective index of refraction n_{eff} and absorption index k_{eff} as functions of the ratio L/D for a porosity ϕ equal to 0.1963. The thick solid line corresponds to the predictions of the VAT models given by Eqs. (12) and (13). The data points represent the values retrieved from the numerically computed transmittance by minimizing δT . As established for nonabsorbing thin films,²⁴ the effective index of refraction n_{eff} as well as the effective absorption index k_{eff} become independent of both the film thickness and the pore diameter for

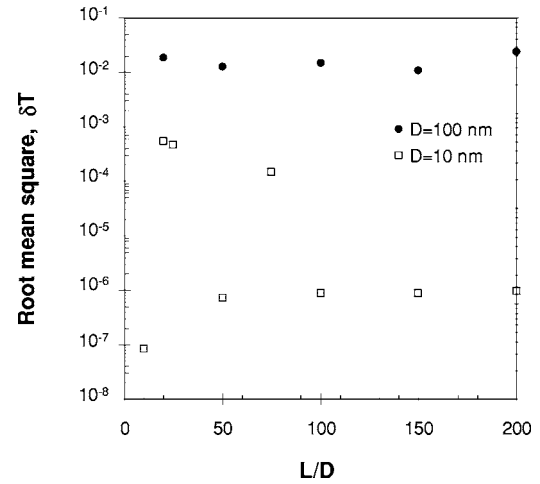


FIG. 3. Root mean square δT as calculated according to Eq. (24) as a function of L/D .

thick enough films corresponding to $L/D > 100$ in the cases investigated. In addition, for porosity $\phi=0.1963$, the VAT model predicts the retrieved values of n_{eff} and k_{eff} for $L/D = 200$ within 0.13% and 0.075%, respectively. Finally, Fig. 3 shows the root mean square δT as a function of the ratio L/D . The value of δT remains small and decreases as the film thickness increases due to smoother interference fringes. It also decreases as the bubble diameter decreases thanks to reduction in scattering by the bubbles. For most cases (except for $L/D < 20$ and $D=100\text{nm}$), the numerical and calculated transmittances T_{num} and T_{calc} plotted for wavelengths between 400 and 900 nm are undistinguishable. For example, for $D=10\text{nm}$, $L/D=150$, and $\phi=0.3$, the maximum relative error $|T_{\text{num}} - T_{\text{calc}}|/T_{\text{num}}$ is 0.07% while δT is equal to 2.04×10^{-4} . Note also that (i) all numerical results were converged, i.e., independent of the number of meshes and (ii) the root mean square remains relative small. Thus, the large variations in n_{eff} and k_{eff} observed for small values of L/D are attributed to interferences between nanopores whose effect tend to average out once enough pores are considered. Then, beyond a critical film thickness to pore diameter ratio, the medium behaves as homogeneous with some effective properties.

Moreover, Fig. 4 compares the predictions of various effective medium approaches applied to the through-plane effective index of refraction n_{eff} and absorption index k_{eff} of nanoporous thin films as a function of porosity for $n_c = 1.44$, $k_c=0.01$, $n_d=1.0$, $k_d=0.0$, $D=10\text{ nm}$, and $L/D = 150$. Note that the series and reciprocity models cannot be computed for k_{eff} because $k_d=0.0$. As intuitively expected, n_{eff} and k_{eff} decrease as the porosity increases. Overall, good agreement is found between the VAT model and the numerical results while the parallel, series, Maxwell-Garnett, and reciprocity models applied to n_{eff} and k_{eff} underpredict the numerical values. The same conclusions were obtained when considering the effective index of refraction of nonabsorbing nanoporous thin films.²⁴ Note that the values of n_{eff} predicted by the Lorentz-Lorenz equation [Eq. (39)] fell within 0.2% of the predictions of the Maxwell-Garnett model and, therefore, were omitted in Fig. 4 for the sake of clarity. In addi-

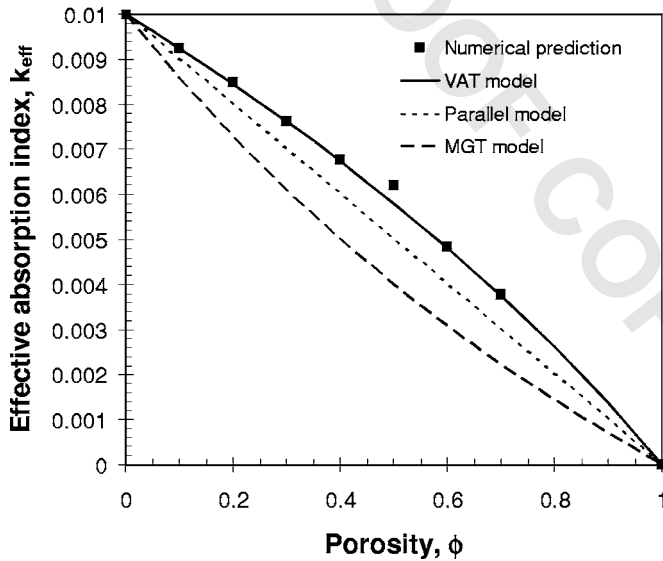
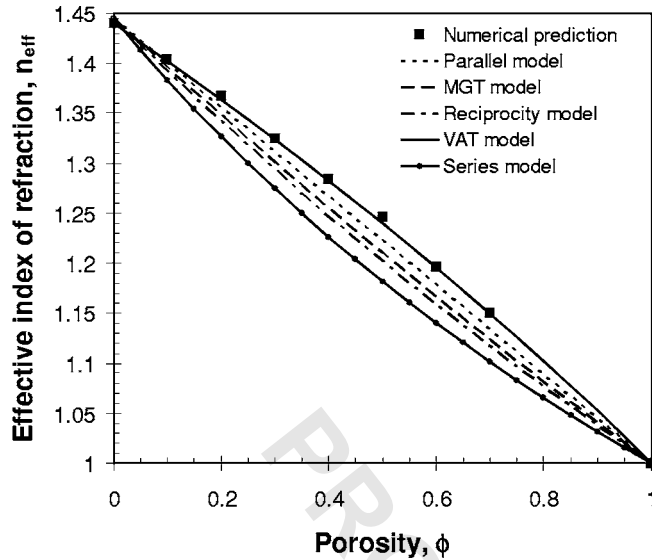


FIG. 4. Evolution of the through-plane effective index of refraction and absorption index as a function of porosity for nanoporous thin films with $n_c=1.44$, $k_c=0.01$, $n_d=1.0$, $k_d=0.0$, $D=10$ nm, and $L/D=150$.

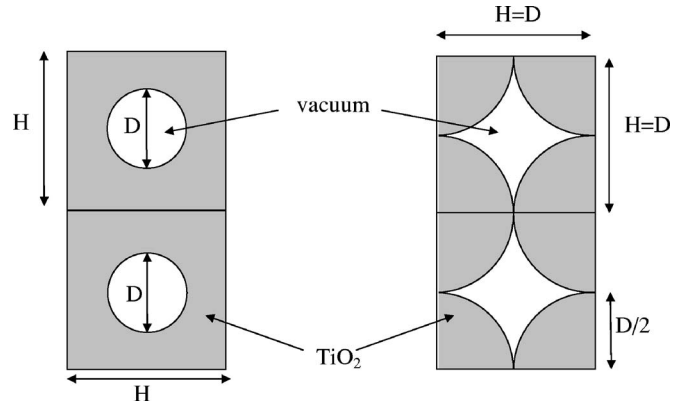


FIG. 5. Morphology of simulated nanoporous with cylindrical nanopores (left) or nanowires (right) for $\phi=0.2146$.

$$n_{c,\lambda} = 2.179 - 3.234 \times 10^{-4}\lambda + 7.967 \times 10^{-8}\lambda^2, \quad (28) \quad 409$$

$$k_{c,\lambda} = 8.501 \times 10^{-4} + 1.264 \times 10^{-5}\lambda - 9.362 \times 10^{-9}\lambda^2, \quad (29) \quad 410$$

where the wavelength λ is expressed in nanometers and varies between 400 and 900 nm. First, the transmittance and reflectance computed for cylindrical pores embedded in a TiO_2 matrix and for cylindrical TiO_2 nanowires (Fig. 5) were found to be identical. This indicates that beyond a critical film thickness, the pore shape has no effect on the effective optical properties of the nanocomposite materials as found by Braun and Pilon²⁴ for nonabsorbing nanoporous thin films. Note that the top surface of the thin film is optically smooth and the film surface roughness due to the presence of nanowires is not accounted for.

Finally, the theoretical transmittance and reflectance were computed using Eqs. (25) and (27) for an homogeneous thin film having effective spectral index of refraction and absorption index predicted by the VAT model [Eqs. (12) and (15)]. Figure 6 shows good agreement between the numerical and theoretical transmittances and reflectances of a nanoporous TiO_2 thin film of porosity 0.2146. The maximum absolute errors in transmittance and reflectance were less than 0.03% and 0.0065%, respectively, and an average relative error less than 3.0%. This confirms the validity of the VAT model on a spectral basis for the effective complex refraction of nanoporous media consisting of cylindrical pores in an absorbing matrix or of closely packed nanowires.

B. Dielectric medium with metallic nanowires 435

This section aims at assessing the validity of the VAT model for dielectric materials or fluids containing metallic nanowires. Let us consider a dielectric continuous phase of complex index of refraction $m_c=1.4-i0.0$ containing gold nanowires and having the same index of refraction as bulk gold at 400 nm, i.e., $m_d=1.66-i1.96$.²³ Two nanowire diameters D are considered namely 10 and 100 nm and, in all cases, the overall film thickness L is such that $L/D=150$. Then, the film can be treated as homogeneous and effective properties can be defined.

tion, when the pores are open and consist of a set of alternating columns of dispersed and continuous phase, perpendicular to the substrate, the dielectric constant can be modeled using the parallel model given by Eq. (7).³⁰ Therefore, the VAT model for both n_{eff} and k_{eff} provides an accurate prediction of the effective optical properties of the nanoporous thin films simulated with various pore sizes and porosities. The other effective property models appear not to be appropriate for the reasons previously discussed.

In addition, spectral calculations for nanoporous TiO_2 over the spectral range from 400 to 900 nm have been performed for cylindrical nanopores and nanowires of diameter $D=10$ nm and for porosity of 0.2146 as illustrated in Fig. 5. The overall film thickness L was such that $L/D=150$ to ensure that the heterogeneous thin film behaves as homogeneous with some effective properties. The spectral dependency of the complex index of refraction of bulk TiO_2 was accounted for by fitting reported experimental data^{39,40} with a second-order polynomial to yield

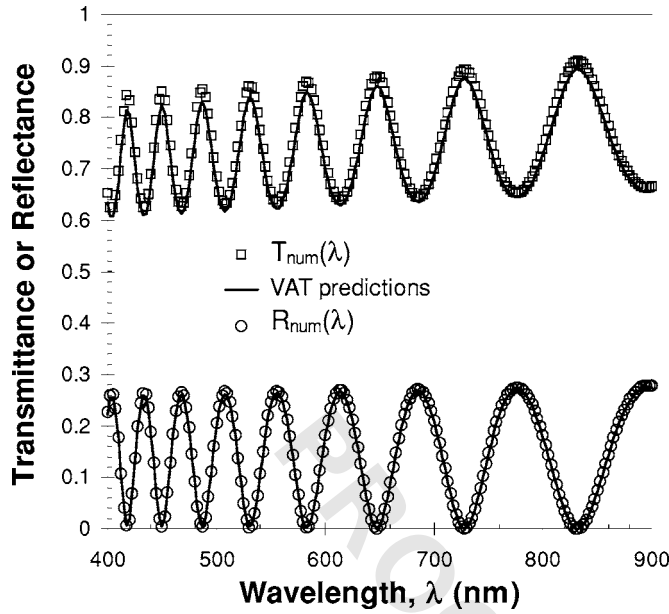


FIG. 6. Comparison of theoretical and numerical spectral transmittance and reflectance of nanoporous TiO_2 with cylindrical nanopores and nanowires of diameter $D=10$ nm and porosity $\phi=0.2146$ over the wavelength range between 400 and 900 nm and film thickness $L=150 D$.

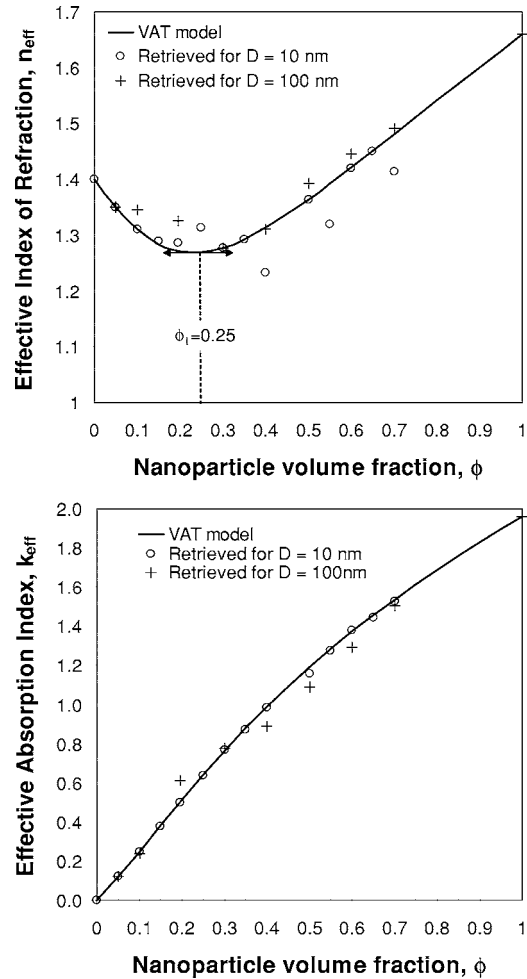


FIG. 7. Comparison between the VAT model and numerically retrieved effective index of refraction and absorption index of dielectric medium ($m_c = 1.4 - i0.0$) with embedded metallic nanowires ($m_d = 1.66 - i1.96$) for various volume fractions and nanowire diameter.

requires that the size parameter $\chi = \pi D / \lambda$ be much smaller 481 than unity.⁴¹ This assumption is typically valid for absorbing 482 nanocomposite materials and nanofluids in the visible and 483 infrared part of the spectrum. In the present study χ varies 484 between 0.011 and 0.25. In estimating T_{calc} and R_{calc} from the 485 EM wave theory, the fraction of energy scattered by nanopores 486 or nanowires was neglected compared with that transmitted 487 and reflected by the film along the incident direction. 488 This assumption was confirmed numerically for all reported 489 results by comparing the magnitude of the y component of the 490 Poynting vector perpendicular to the incident directions 491 with its x component at all locations in the x - y plane, i.e., 492 $|\pi_y|_{\text{avg}} \ll |\pi_x|_{\text{avg}}$. 493

C. Discussion of the effective VAT model 494

The objective of this section is to mathematically ana- 495 lyze the now numerically validated expressions of n_{eff} and 496 k_{eff} given by Eqs. (12) and (13). Their derivatives with re- 497 spect to volume fraction ϕ are expressed as 498

$$\frac{\partial n_{\text{eff}}^2}{\partial \phi} = \frac{1}{2} [\alpha + (A^2 + B^2)^{-1/2} (A\alpha + B\beta)], \quad (30) \quad 499$$

446 Figure 7 compares the through-plane effective index of 447 refraction and absorption index of the nanocomposite me- 448 dium retrieved from both numerical transmittance and reflec- 449 tance with those predicted by the VAT model for volume 450 fraction of nanowires ϕ ranging from 0.0 to 0.7. Note that 451 the retrieved effective optical properties were obtained by 452 minimizing $\delta T + \delta R$ and were very sensitive to the initial 453 guess particularly for $D=100$ nm when transmittance was 454 very small. In those cases, the properties were retrieved by 455 minimizing only the root mean square δR . Overall, there 456 exist a relatively good agreement between the retrieved val- 457 ues of n_{eff} and k_{eff} at all nanowire volume fractions and for 458 both $D=10$ and 100 nm. The VAT model predicts the re- 459 trieved effective index of refraction n_{eff} within $\pm 6.2\%$ and 460 the effective absorption index k_{eff} within $\pm 2.9\%$. The fact 461 that metallic nanowires have size dependent optical proper- 462 ties has been ignored but can be accounted for provided that 463 these properties be measured independently.

464 Moreover, it is interesting to note that the presence of a 465 strongly absorbing dispersed phase such as metallic nano- 466 wires reduces dramatically the effective index of refraction 467 of the composite medium even for small volume fractions ϕ . 468 For certain values of ϕ , the effective index of refraction n_{eff} 469 is smaller than that of either the continuous or dispersed 470 phases, i.e., $n_{\text{eff}} \leq \text{Min}(n_c, n_d)$. It also reaches a minimum at 471 the volume fraction $\phi_1 = 0.25$ as discussed in detail in the 472 next section. Simultaneously, the effective absorption index 473 increases significantly even for small metallic nanowire vol- 474 ume fractions. Note also that if the film is thick enough for 475 the effective medium approximation to be valid, the metallic 476 nanowires can take various shapes and/or sizes without af- 477 fecting the above predictions.

478 Finally, scattering by the nanopores and nanoparticles 479 can be neglected if their size is much smaller than the wave- 480 length of the incident radiation.^{41,42} A quantitative criterion

500
$$\frac{\partial k_{\text{eff}}^2}{\partial \phi} = \frac{1}{2}[-\alpha + (A^2 + B^2)^{-1/2}(A\alpha + B\beta)], \quad (31)$$

501 where

502
$$\alpha = \frac{\partial A}{\partial \phi} = (n_d^2 - k_d^2) - (n_c^2 - k_c^2)$$

503 and

504
$$\beta = \frac{\partial B}{\partial \phi} = 2(n_d k_d - n_c k_c). \quad (32)$$

505 Note that the derivatives of A and B with respect to porosity
506 ϕ denoted by α and β , respectively, are independent of po-
507 rosity. The effective properties n_{eff} and k_{eff} reach their maxi-
508 mum or minimum when the first-order derivatives with re-
509 spect to volume fraction vanish, i.e., when

510
$$(A^2 + B^2)^{-1/2}(A\alpha + B\beta) = -\alpha \quad (33)$$

511 and

512
$$(A^2 + B^2)^{-1/2}(A\alpha + B\beta) = \alpha. \quad (34)$$

513 Squaring both sides of Eqs. (33) and (34) yields the same
514 second-order polynomial in terms of the volume fraction ϕ .
515 Given the complex index of refraction of both phases, one
516 can solve for the critical volume fraction corresponding to a
517 minimum and/or maximum of the effective index of refrac-
518 tion and/or absorption index. After rearrangement two roots
519 ϕ_1 and ϕ_2 can be found

520
$$\phi_1 = \frac{2[(\alpha^2 - \beta^2)n_c k_c - \alpha\beta(n_c^2 - k_c^2)]}{\beta(\alpha^2 + \beta^2)}, \quad (35)$$

521
$$\phi_2 = \frac{n_c k_c}{n_c k_c - n_d k_d}. \quad (36)$$

522 In order to know whether n_{eff} and k_{eff} reach their maximum
523 or minimum, their second-order derivatives with respect to ϕ
524 have to be examined. Based on Eqs. (33) and (34), the
525 second-order derivatives of n_{eff} or k_{eff} are the same for ϕ_1
526 and ϕ_2 and can be expressed as

527
$$\left. \frac{\partial^2 n_{\text{eff}}}{\partial \phi^2} \right|_{\phi_{1,2}} = \frac{1}{4n_{\text{eff}}} \frac{(A\beta - B\alpha)^2}{(A^2 + B^2)^{3/2}}, \quad (37)$$

528
$$\left. \frac{\partial^2 k_{\text{eff}}}{\partial \phi^2} \right|_{\phi_{1,2}} = \frac{1}{4k_{\text{eff}}} \frac{(A\beta - B\alpha)^2}{(A^2 + B^2)^{3/2}}. \quad (38)$$

529 Since the terms on the right-hand side of the above two equa-
530 tions are always positive, n_{eff} and k_{eff} can only reach a mini-
531 mum.

532 However, for an arbitrary set of dispersed and continu-
533 ous phases, the values of ϕ_1 and ϕ_2 do not always fall in the
534 physically acceptable range of porosities between 0 and 1.
535 For positive values of the properties n_c , n_d , k_c , and k_d , one
536 can show that, unlike ϕ_1 , the second root ϕ_2 never falls
537 between 0 and 1.

538 Moreover, the following expressions can be used to
539 identify whether ϕ_1 is the solution of Eqs. (33) or (34), i.e.,
540 whether n_{eff} or k_{eff} reach a minimum at $\phi = \phi_1$

$$\chi = \frac{n_d k_d - n_c k_c}{n_c k_c (n_d^2 - k_d^2) - n_d k_d (n_c^2 - k_c^2)}. \quad (39) \quad 541$$

If χ is strictly positive then k_{eff} reaches a minimum while n_{eff}
reaches a minimum if χ is strictly negative. Neither n_{eff} nor
 k_{eff} reach a minimum if $\chi=0$. In the case of nanoporous
media, χ and ϕ_2 are constant and equal to -1 and 1 , respec-
tively. Therefore n_{eff} can reach a minimum less than 1.0 at an
acceptable ϕ_1 . Finally, for the dielectric medium with em-
bedded metallic nanowires simulated previously, χ is strictly
negative and n_{eff} reaches a minimum. This is illustrated in
Fig. 7 where n_{eff} reaches a minimum of 1.33 at $\phi_1=0.25$.

Finally, this study constitutes the first two-dimensional
numerical validation for TE polarization of the VAT applied
to the three-dimensional Maxwell equations^{28,29} in two-phase
systems with dispersed domains of arbitrary shape. For com-
plete validation, the present study should be extended to both
a three-dimensional and transverse magnetic (TM) polariza-
tion cases.

V. CONCLUSIONS

The VAT models for the effective dielectric and electri-
cal properties of two-phase media²⁸ have been used to derive
the through-plane effective index of refraction n_{eff} and ab-
sorption index k_{eff} of nanoporous materials. Moreover, a nu-
merical scheme has been developed and implemented to
solve the Maxwell equations for a normally incident TE elec-
tromagnetic wave traveling through (1) nanoporous SiO_2 and
 TiO_2 consisting of cylindrical pores or nanowires and (2)
dielectric medium containing cylindrical nanowires. All in-
terfaces were treated as optically smooth and the dispersed
phase volume fraction varied from 0.0 to 0.7 . Calculations
were performed on a gray or spectral basis between 400 and
 900 nm. The effective optical properties for the simulated
nanocomposite thin films were retrieved by minimizing the
root mean square of the relative errors for the transmittance
and reflectance. In all cases, the results for both k_{eff} and n_{eff}
are in good agreement with the predictions from the VAT
model. Finally, the numerically validated VAT model is dis-
cussed and used to predict the behavior of the optical prop-
erties of nanocomposite materials. It shows that under certain
conditions, the effective index of refraction or absorption
index of the composite material can be smaller than that of
both the continuous and dispersed phases. The same results
and conclusions are expected for spherical pores and nano-
particles. These results can be used to design and optimize
nanocomposite materials with tunable optical properties. As
well as to measure the porosity or nanowire volume fraction
provided that the film be thick enough to be treated as ho-
mogeneous with some effective properties and that all sur-
faces be optically smooth.

ACKNOWLEDGMENTS

This work was supported by the National Science Foun-
dation through the CAREER Award Program (CTS 0449429)
and by Intelligent Optical Systems, Inc., Torrance, CA.

¹C. J. Brinker, Y. Lu, A. Sellinger, and H. Fan, Adv. Mater. (Weinheim, 593

- 594 Ger.) **11**, 579 (1999).
 595 ²H. Fan, H. R. Bentley, K. R. Kathan, P. Clem, Y. Lu, and C. J. Brinker, *J.*
 596 *Non-Cryst. Solids* **285**, 79 (2001).
 597 ³P. C. A. Alberius, K. L. Frindell, R. C. Hayward, E. J. Kramer, G. D.
 598 Stucky, and B. F. Chmelka, *Chem. Mater.* **14**, 3284 (2002).
 599 ⁴B. W. Eggiman, M. P. Tate, and H. W. Hillhouse, *Chem. Mater.* **18**, 723
 600 (2006).
 601 ⁵B. O'Regan and M. Grätzel, *Nature* **353**, 737 (1991).
 602 ⁶P. Ravirajan, S. A. Haque, D. Poplavskyy, J. R. Durrant, D. D. C. Bradley,
 603 and J. Nelson, *Thin Solid Films* **451–452**, 624 (2004).
 604 ⁷L. Schmidt-Mende and M. Grätzel, *Thin Solid Films* **500**, 296 (2006).
 605 ⁸M. I. Sanchez, J. L. Hedrick, and T. P. Russell, *J. Polym. Sci., Part B:*
 606 *Polym. Phys.* **33**, 253 (1995).
 607 ⁹M. I. Sanchez, J. L. Hedrick, and T. P. Russell, in *Microporous and*
 608 *Macroporous Materials Materials Research Society Symposium Proceed-*
 609 *ings* (Materials Research Society, Pittsburgh, PA, 1996), Vol. 431, pp.
 610 475–480.
 611 ¹⁰R. J. Martin-Palma, V. Torres-Costa, M. Arroyo-Hernandez, M. Manso, J.
 612 Perez-Rigueiro, and J. M. Martinez-Duart, *Microelectron. J.* **35**, 45
 613 (2004).
 614 ¹¹M. Arroyo-Hernandez, R. J. Martin-Palma, J. Perez-Rigueiro, J. P. Garcia-
 615 Ruiz, J. L. Garcia-Fierro, and J. M. Martinez-Duart, *Mater. Sci. Eng., A*
 616 **23**, 697 (2003).
 AQ: ¹²S. Chan, Y. Li, L. J. Rothberg, B. L. Miller, and P. M. Fauchet, *Mater. Sci.*
 #4 ¹³Eng., A **15**, 277 (2001).
 619 ¹³A. Loni, L. T. Canham, M. G. Berger, R. Arens-Fischer, H. Munder, H.
 620 Luth, H. F. Arrand, and T. M. Benson, *Thin Solid Films* **276**, 143 (1996).
 621 ¹⁴H. F. Arrand, T. M. Benson, A. Loni, M. G. Krueger, M. Thoenissen, and
 622 H. Lueth, *Electron. Lett.* **33**, 1724 (1997).
 623 ¹⁵A. Jain, S. Rogojevic, S. Ponoth, I. Matthew, W. N. Gill, P. Persans, M.
 624 Tomozawa, J. L. Plawsky, and E. Simonyi, *Thin Solid Films* **398–399**,
 625 513 (2001).
 626 ¹⁶M. G. Berger, M. Thonissen, R. Arens-Fischer, H. Munder, H. Luth, M.
 627 Arntzen, and W. Thei, *Thin Solid Films* **255**, 313 (1995).
 628 ¹⁷J. Diener, N. Künzner, D. Kovalev, E. Gross, V. Y. Timoshenko, G. Po-
 629 lisski, and F. Koch, *Appl. Phys. Lett.* **78**, 3887 (2001).
 630 ¹⁸M. Krüger, M. Marso, M. G. Berger, M. Thönissen, S. Billat, R. Loo, W.
 631 Reetz, H. Lüth, S. Hilbrich, R. Arens-Fischer, and P. Grosse, *Thin Solid*
Films **297**, 241 (1997).
 632 ¹⁹S. Zangoie, M. Schubert, C. Trimble, D. W. Thompson, and J. A. Wool-
 633 lam, *Appl. Opt.* **40**, 906 (2001).
 634 ²⁰S. Zangoie, R. Jansson, and H. Arwin, *J. Appl. Phys.* **86**, 850 (1999).
 635 ²¹C. Mazzoleni and L. Pavesi, *Appl. Phys. Lett.* **67**, 2983 (1995).
 636 ²²K. Kordás, S. Beke, A. E. Pap, A. Uusimäki, and S. Leppävuori, *Opt.*
 637 *Mater.* **25**, 257 (2004).
 638 ²³M. Q. Brewster, *Thermal Radiative Transfer and Properties* (Wiley-
 639 Interscience, New York, 1992).
 640 ²⁴M. Braun and L. Pilon, *Thin Solid Films* **496**, 505 (2006).
 641 ²⁵J. C. M. Garnett, *Philos. Trans. R. Soc. London, Ser. A* **203**, 385 (1904).
 642 ²⁶D. A. G. Bruggeman, *Ann. Phys.* **24**, 636 (1935).
 643 ²⁷J. A. del Rio, R. W. Zimmerman, and R. A. Dawe, *Solid State Commun.*
 644 **106**, 183 (1998).
 645 ²⁸J. A. de Río and S. Whitaker, *Transp. Porous Media* **39**, 159 (2000).
 646 ²⁹J. A. Rio and S. Whitaker, *Transp. Porous Media* **39**, 259 (2000).
 647 ³⁰M. Braun, "Effective optical properties of nanoporous thin-films," M.S.
 648 thesis, Mechanical and Aerospace Engineering Department, University of
 649 California, Los Angeles, CA, 2004.
 650 ³¹K. Postava and T. Yamaguchi, *J. Appl. Phys.* **89**, 2189 (2001).
 651 ³²B. Sareni, L. Krähenbühl, and A. Beroual, *J. Appl. Phys.* **80**, 1688 (1996).
 652 ³³FEMLAB 3 Electromagnetics Module User's Guide, Version 3.0, Comsol
 653 AB, 2004.
 654 ³⁴A. E. Pap, K. Kordás, J. Vähäkangas, A. Uusimäki, S. Leppävuori, L.
 655 Pilon, and S. Szatmári, *Opt. Mater. (Amsterdam, Neth.)* **28**, 506 (2006).
 656 ³⁵P. Ferrand and R. Romestain, *Appl. Phys. Lett.* **77**, 3535 (2000).
 657 ³⁶G. Lerondel and R. Romestain, *Thin Solid Films* **297**, 114 (1997).
 658 ³⁷L. S. Lasdon, A. D. Waren, A. Jain, and M. Ratner, *ACM Trans. Math.*
 659 *Softw.* **4**, 34 (1978).
 660 ³⁸M. F. Modest, *Radiative Heat Transfer* (McGraw-Hill, New York, 2002).
 661 ³⁹C. J. Brinker and C. W. Scherer, in *Sol-Gel Science* (Academic, San
 662 Diego, 1990), p. 803C.
 663 ⁴⁰G. Gülşen and M. Naci İnci, *Opt. Mater. (Amsterdam, Neth.)* **18**, 373
 664 (2002).
 665 ⁴¹C. F. Bohren and D. R. Huffman, *Absorption and Scattering of Light by*
 666 *Small Particles* (Wiley-Interscience, New York, 1983).
 667 ⁴²R. Viskanta and M. P. Mengüç, *Appl. Mech. Rev.* **42**, 241 (1989).
 668

AUTHOR QUERIES — 218624JAP

- #1 Q1: PROOFREADING: Do not change PHI's throughout article even though the ones in the Xyvision proof are different than the ones on the hardcopy. THIS IS OKAY TO LEAVE AS IS! Thanks!
- #2 Author: Please check wording – transmitted film?
- #3 Ref. 39 was not cited in text. Please check our citation and fix if necessary.
- #4 Refs. 11 and 12: please check journal title. Is it A or B?

PROOF COPY 218624JAP